THE JOURNAL OF PHYSICAL CHEMISTRY C

Article

Supramolecular Interactions of Chenodeoxycholic Acid Increase the Efficiency of Dye-Sensitized Solar Cells Based on a Cobalt Electrolyte

Paolo Salvatori, Gabriele Marotta, Antonio Cinti, Chiara Anselmi, Edoardo Mosconi, and Filippo De Angelis

J. Phys. Chem. C, **Just Accepted Manuscript** • Publication Date (Web): 06 Feb 2013

Supramolecular Interactions of Chenodeoxycholic Acid Increase the Efficiency of Dye-Sensitized Solar Cells Based on a Cobalt Electrolyte

Paolo Salvatori,[a,b] *Gabriele Marotta,* [a,b] *Antonio Cinti,* [a,b] *Chiara Anselmi,* [a] *Edoardo Mosconi,*[a,*] *Filippo De Angelis* [a,*]

[a] Computational Laboratory fo Hybrid/Organic Photovoltaics (CLHYO), Istituto CNR di Scienze e Tecnologie Molecolari (ISTM-CNR), Via elce di Sotto 8, I-06213, Perugia, Italy.

[b] Department of Chemistry, University of Perugia, Via elce di Sotto 8, I-06213, Perugia, Italy.

Corresponding author: Filippo De Angelis, Computational Laboratory fo Hybrid/Organic Photovoltaics (CLHYO), Istituto CNR di Scienze e Tecnologie Molecolari (ISTM-CNR), Via elce di Sotto 8, I-06213, Perugia, Italy. Telephone: +390755855523. E-mail: filippo@thch.unipg.it

RECEIVED DATE (to be automatically inserted after your manuscript is accepted if required according to the journal that you are submitting your paper to)

ABSTRACT

A combined experimental and computational study is carried out to understand the nature of the interfaces between dye-sensitized TiO_2 and cobalt-based electrolyte in the presence of a prototype co-absorbent, chenodeoxycholic acid (CDCA), employed in Dye-Sensitized Solar Cells (DSCs). It was recently reported that including CDCA both in the dye *and* in the electrolyte solutions substantially improved the performance of DSCs based on a Fc/Fc^+ electrolyte (Daeneke et al. *Nat. Chem.* **2011,** *3*,1755) . Here we evaluate the individual and combined effect of CDCA as a surface co-adsorbent and as an additive in DSCs based on a Co(II)/Co(III) electrolyte, in combination with two prototypical Ru(II) dyes, N719 and Z907. For both dyes, the concomitant use of CDCA in the dye bath and in the electrolyte solution leads to a significant improvement, by ca. a factor 2, of the DSCs photovoltaic performances, allowing us to reach 5.3% efficiency with Z907. FT-IR analyses conducted on the solid and TiO_2-adsorbed CDCA highlight the presence of surface-adsorbed interacting CDCA molecules, possibly creating a bulky insulating network on the TiO_2 surface. Computational analyses have been carried out to gain insight into the nature of the supramolecular aggregates occurring for CDCA on the TiO_2 surface.

KEYWORDS:

DSCs; CDCA; DFT calculations; recombination

1. Introduction

Dye-sensitized Solar Cells (DSCs) represent a promising approach to the direct conversion of sunlight into electrical energy at low cost and with high efficiency.[1 2, 3 4] This has been very recently demonstrated by the launch of the first DSC-based commercial product. DSCs are based on a dye-sensitized mesoporous oxide layer, usually composed by a network of sintered nanoparticles (typically anatase TiO_2 ~20-30 nm diameter), interpenetrated by a liquid redox electrolyte (typically I^-/I_3^- or Co(II)/Co(III)-polypiridine complexes in a volatile organic solvent), Scheme 1. Upon photoexcitation of the chemisorbed dye, charge separation occurs at the dye-sensitized semiconductor interface and electrons are injected into the oxide conduction band (CB); the generated charges travel across the TiO_2 nanoparticle network and can be collected at the transparent conducting glass back contact. The oxidized dye is regenerated by the redox shuttle electrolyte. The circuit is closed by electrolyte regeneration at the counter-electrode, see Scheme 1.

The iodide/triiodide (I^-/I_3^-) redox couple has maintained a clear lead in DSCs for many years,[5] although this system is now being rivaled by the Co(II)/Co(III),[6-9] Cu(I)/Cu(II),[10] and Fe(II)/Fe(III)[11] redox couples. As a matter of fact, the record DSCs efficiency to date has been obtained by a Co(II)/Co(III) liquid electrolyte.[8]

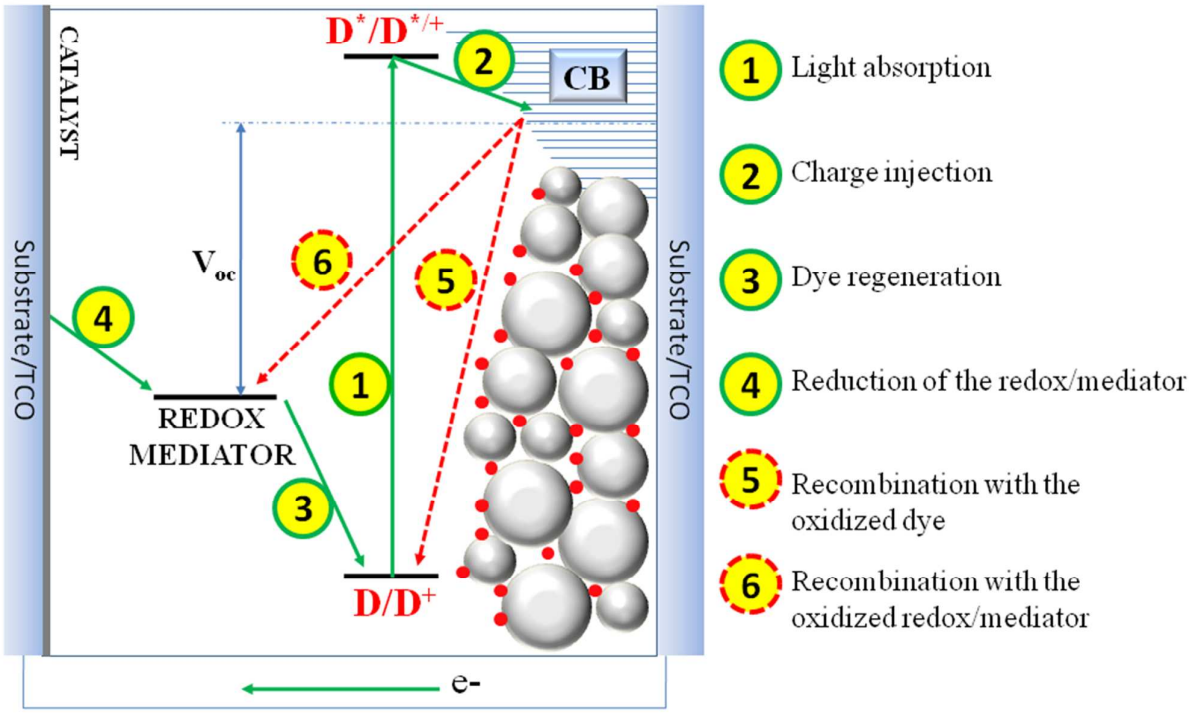

Scheme 1. Schematic representation of the constituent materials and energy levels of a DSC along with forward (green lines) and backward (dotted red lines) electronic processes. The energy levels roughly correspond to those of a DSC based on the N3 dye (red spots), TiO_2 nanoparticles (grey spheres) and I^-/I_3^- redox mediator (not shown).

The DSCs efficiency is the product of the short-circuit photocurrent density (J_{sc}), the open circuit voltage (V_{oc}) and the cell fill-factor (ff) divided by the intensity of the incident light (Is), namely:

$$\eta = J_{sc} \times V_{oc} \times FF / I_s \qquad (1)$$

The three ingredients of a DSC, namely the dye, the semiconductor oxide and the redox couple, can be individually or simultaneously optimized in search of higher efficiencies. The photocurrent density is directly related to the charge generation and collection efficiency, which in

turn depend upon the dye light-harvesting and the kinetics of electron injection, dye regeneration and charge transport within the cell. As such, a sizable contribution to J_{sc} depends directly on the dye. The DSCs open circuit voltage represents the difference between the quasi-Fermi level of the semiconductor under illumination and the redox potential of the redox shuttle electrolyte, see Scheme 1, the latter being nearly constant under operation conditions due to the high concentration of redox species. The quasi-Fermi level ($E_{F,n}$) of the semiconductor depends "statically" on the semiconductor conduction band (CB) energy and "dynamically" on the charge density (n) accumulated in the semiconductor, [7] according to the following equation:

$$E_{F,n}=E_{CB}+k_BT \ln[n/N_c] \quad (2)$$

where N_c is the density of states in the semiconductor. Accordingly, a higher semiconductor CB and charge density accumulation in the semiconductor provide a raise of the quasi-Fermi level and thus of the V_{oc}. At the same time, a more positive redox shuttle potential leads to increased V_{oc}, Scheme 1. This aspect is exploited in Co(II)/Co(III) electrolytes and in general in transition metal redox shuttle endowed with a tunable redox potential.[12] It is thus clear that V_{oc} depends only *indirectly* on the dye, which can either exert an effect on the TiO_2 CB energy[13] or affect the recombination reactions which vary the charge density into the semiconductor.

The dye chemical nature and structure has been the subject of intensive investigations. Various Ru(II) polypyridyl complexes have primarily been employed as dye sensitizers.[14, 15] The remarkable performance of the N3 dye,[16] of its doubly protonated analogue (N719)[17] and of the so-called black dye[18, 19] led to significant advances of the DSCs technology, with solar to electric power efficiencies exceeding 11%.[20, 21] In the last years, a flourishing family of heteroleptic and cyclometalated Ru(II) dyes have been designed and synthesized to provide higher molar extinction coefficient or peculiar supramolecular interactions compared to N719, thus enhancing the overall

stability and / or efficiency of the DSCs.[19, 22-26] Fully organic sensitizers have also been developed because of their increased molar extinction coefficient, compared to Ru(II)-dyes, spectral tunability and reduced environmental impact,[27, 28] and showed very high photovoltaic efficiencies, exceeding 10%.[29] Finally, functionalized donor-acceptor Zn(II)-porphyrins have recently emerged as a new class of dye sensitizers with high performance, due to the extended absorption spectrum in the red to near IR, region.[30, 31]

TiO_2 is essentially established as the most performing semiconductor metal oxide in DSCs, both in the form of the commonly employed sintered nanoparticles or nanotubes,[32-34] although research on alternative oxides is also actively pursued.[35-39]

The I^-/I_3^- redox couple in an organic solvent has been considered as the standard high-performance electrolyte in DSCs for many years; all champion DSCs reported up to 2010 were based on such redox couple.[19, 26] Solid state DSCs based on the spiro-OMeTAD solid hole conductor are also actively investigated, delivering top efficiencies of about 7%.[40, 41] Although highly performing, the I^-/I_3^- redox couple has several disadvantages, including its high corrosivity towards most of noble metals, except gold, which imposes stringent requisites to DSCs module fabrication. Also, the unfavorable thermodynamics of its complex two-electron redox cycle implies DSCs voltage losses of ca. 600 mV,[5] mainly related to the dye regeneration process.[42] The two-electron / bimolecular nature of the recombination pathway between injected electrons and the oxidized dye or oxidized species in the electrolyte is a key to suppress such parasitic processes, which would reduce both V_{oc} and J_{sc}.[5, 43]

Various attempts have been made to replace the I^-/I_3^- redox couple by alternative electrolytes based on simpler one-electron redox couples, although the high recombination rates typical of such systems has prevented for a long time to achieve high photovoltaic performances. Among the systems which have been experimented, we mention Co(II)/Co(III) polypiridyl complexes,[6-9, 44-50] Fe(II)/Fe(III) ferrocene/ferrocenium complexes,[11, 40, 51, 52] Cu(I)/Cu(II) complexes, [10, 53] organic

redox couples,[54, 55] CuNCS[56, 57] and S^-/S_2^- redox couples, the latter being largely employed in quantum dot-based DSCs.[58, 59] Very interestingly, the investigated transition metal complexes have tunable redox potentials which can be pushed up to ca. 1 V vs. SHE, so that if efficient charge collection can be achieved, a correspondingly higher V_{oc} might be extracted. Maintaining the same J_{sc} and FF of champion DSCs based on I^-/I_3^-, this readily translates into overall device efficiencies approaching 15%.

Despite the great potential for alternative redox couple, only very recently these systems have started delivering high DSCs efficiencies. An emblematic case in this respect is that recently reported by Daeneke *et al.* for the ferrocene/ferrocenium (Fc/Fc^+) electrolyte,[11] which in conjunction with a specifically tailored organic dye, reached 7.5 % efficiency. The key to such a high efficiency was the peculiar dye structure, which probably prevented the oxidized Fc^+ to approach the TiO_2 surface, thus substantially reducing parasitic recombination reactions. Also in the case of Co(II)/Co(III) electrolytes it is evident in the literature the key role of the blocking dye chains in shielding the TiO_2 surface and limiting the recombination of the injected electrons with the oxidized form of the redox couple.[60] All the most performing dyes in the cobalt-based DSCs are now designed with bulky alkyl or alkoxy chains.[6, 8, 9]

A further interesting aspect of the work by Daeneke *et al.* [11] lies in the observation that including the prototype chenodeoxycholic acid co-adsorbent both in the dye *and* in the electrolyte solution substantially improved the DSCs performance, both in terms of V_{oc} and J_{sc}. This unprecedented observation deserves, in our opinion, further attention, since it might be a key to further expanding the applicability of alternative redox couples for high performance DSCs.

Chenodeoxycholic acid, Scheme 2, hereafter CDCA, is widely used as an anti-aggregant co-adsorbent in DSCs.[61-67] CDCA is employed in variable concentrations in the semiconductor dyeing process and is co-adsorbed on the TiO_2 surface along with the dye to minimize dye/dye intermolecular interactions which may negatively affect the DSCs performances.[68-71] It was also

proposed that acidic co-adsorbents, such as CDCA, may act as a proton buffer for the dye, thus "regulating" the dye proton content and assisting dye adsorption onto the semiconductor surface.[72]

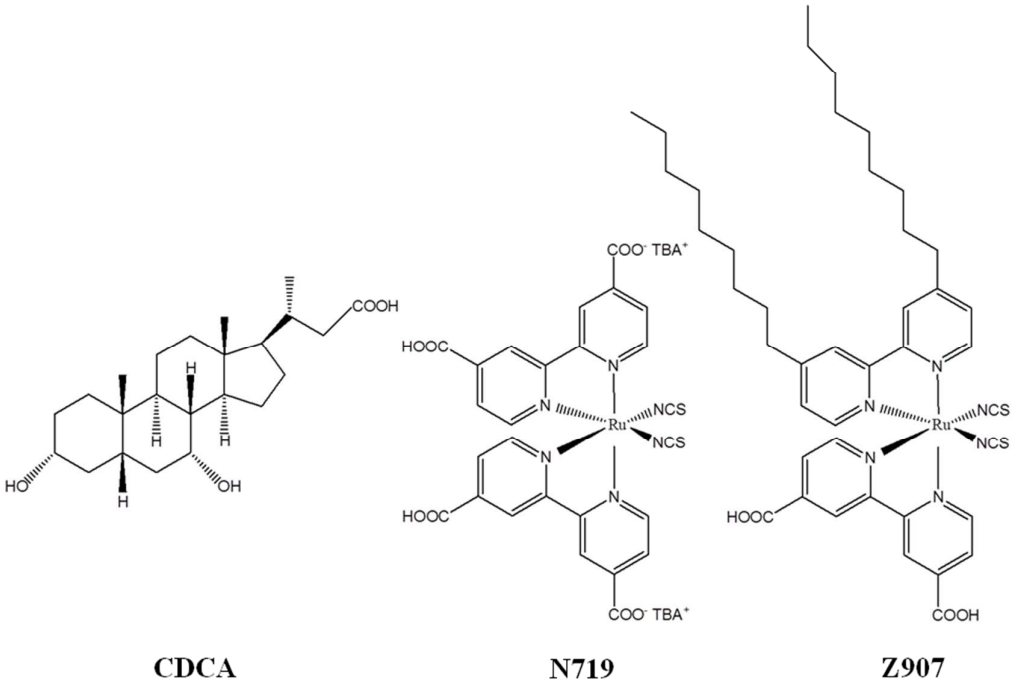

Scheme 2. Molecular structure of Chenodeoxycholic acid (CDCA), N719 and Z907 dyes.

To the best of our knowledge, the effect of CDCA in the electrolyte has not been investigated beyond the work by Daeneke *et al.* in Ref. [11], where a "hermetic protection through the establishment of a steady-state equilibrium between surface adsorbed and electrolyte-borne molecules" was invoked to explain the improved performances. Considering the need to block the approach of Fc^+ to the semiconductor surface to obtain high performances, a tentative explanation of this behavior may lay in supramolecular interactions occurring between CDCA molecules co-adsorbed along with the dye onto the semiconductor surface, and free CDCA molecules present in the electrolyte solution. Inspection of the CDCA chemical structure, Scheme 2, reveals the presence of two OH groups in positions 3a and 7a, which might undergo hydrogen bonding with the carboxylic group and / or with the same OH groups of a different CDCA molecule. The existence of

this kind of interactions, involving a large number of molecules, is confirmed in the solid state by XRD structural determination.[73-76] Furthermore FT-IR and Raman investigations on CDCA, demonstrated the permanence of a similar kernel of interacting molecules, bound via hydrogen bonding, also in $CHCl_3$ solution.[77, 78]

As already reported by Planells et al.[79, 80] supramolecular chemistry can be used to control charge recombination and other reactions in DSCs. Motivated by the observations above, in this paper we evaluate the combined effect of CDCA as a surface co-adsorbent and as an additive in DSCs based on a Co(II)/Co(III) electrolyte, in combination with two prototypical Ru(II) dyes, i.e. N719 and Z907 (Scheme 2). The Z907 dye, which has nonyl chains on one bipyridine ligand, is more effective in shielding the TiO_2 surface from the Co(III) approach, and has shown better performances than N719 in Co(II)/Co(III)-based DSCs.[7] For both dyes, the concomitant use of CDCA in the dye bath and in the electrolyte solution leads to a significant improvement, by ca. a factor 2, of the DSCs photovoltaic performances, allowing us to reach 5.3% efficiency in Z907-based DSCs. FT-IR analyses conducted on the solid and TiO_2-adsorbed CDCA have confirmed the presence of surface-adsorbed interacting CDCA molecules, possibly creating a bulky network also on the TiO_2 surface. A computational model of CDCA adsorption on the TiO_2 surface was then developed to quantify the entity of these supramolecular interactions, in relation to the reported photovoltaic results.

2. Experimental

2.1 Materials

All the materials used in this work were used as received, without further purification, if not stated otherwise. The N719 and Z907 dyes and were purchased from Solaronix, the TiO_2 pastes from Dyesol. $Co[(bpy)_3][PF_6]_2$ and $[Co(bpy)_3][PF_6]_3$ were synthesized following a previously reported procedure.[6] $CoCl_2 \times 6H_2O$ (1.19 g) was dissolved in methanol (15mL). A methanol solution of the

2-2'bipyridine ligand (2.57g in 10mL) was added dropwise while stirring, then the solution was heated (70°C) at reflux for 2h. An excess of ammonium hexafluorophosphate (NH_4PF_6), (1.8g), was added to the solution to form the precipitate. The resulting Co(II) tris-bipyridine complex was finally filtered, washed with ethanol and methanol ad dried under vacuum. Elemental analysis calculated for C30 H24 Co F12 N6 P2: C, 44.08; H, 2.96; N, 10.28%. Found: C, 43.82; H, 3.35; N, 10.37%. Oxidation of the Cobalt(II) complex was performed by adding a slight excess of $NOBF_4$ (10% exceeding the stoichiometric quantity) to an acetonitrile solution of $[Co(bpy)_3][PF_6]_2$. The solvent was then removed by rotary evaporation. The complex was then re-dissolved in acetonitrile, and a large amount of NH_4PF_6 was added to the solution. The final product was precipitated with diethyl ether, filtered and dried under vacuum. Since this is usually a quantitative reaction the product was used without further purification and characterization.

Z907 dye powders were purified by using HPLC (Waters 996, equipped with a photodiode array detector). The dye powder was solubilized in ethanol and injected in the cromatographic column (Phenomenex Jupiter, 10μm, C18, 250mm x 21mm). The mobile phase consisted of distilled acetonitrile with 0.1% of trifluoroacetic acid (CF_3COOH).

2.2 Solar cells fabrication

FTO glass (TEC-15, 2.2 mm thickness, Solaronix) was used for transparent conducting electrodes. The substrate was first cleaned in a ultrasonic bath using a detergent solution, acetone and ethanol respectively (each step 15 min. long). The FTO glass plates were immersed into a 40mM aqueous $TiCl_4$ solution at 70 °C for 30 min and washed with water and ethanol. A layer of transparent TiO_2 paste (18NR-T, Dyesol) was spread on the FTO glass plates by doctor blade. The TiO_2 layer was treated in a ethanol chamber and dried for 5min at 120°C. Then a scattering layer (WER 2.0, Dyesol) was deposited over the transparent layer, by using the same deposition process. The TiO_2 coated electrodes (active area 0.2 cm^2) were gradually heated under air flow at 325 °C for 5 min, at 375 °C for 5 min, at 450 °C for 15 min, and 500 °C for 15 min. After the sintering process, the TiO_2

film was treated with 40mM $TiCl_4$ solution, then rinsed with water and ethanol. The electrodes were heated at 500 °C for 30 min and after cooling (80 °C) were immersed for 20 hours into sensitizing baths. These consisted of EtOH solutions of the N719 and Z907 dyes (Solaronix) in 0.2 mM concentration, and when required with 20.0 mM of 3a,7a-dihydroxy-5b-cholic acid (CDCA) added.

Counter electrodes were prepared by coating with a drop of H_2PtCl_6 solution (2 mg of Pt in 1 mL of ethanol) a FTO plate (TEC 15/2.2 mm thickness, Solaronix) and heating at 400 °C for 15 min. The TiO_2 sensitized photoanode and Pt counter electrode were assembled into a sealed sandwich-type cell by a hot-melt ionomer film (Surlyn, 25 μm thickness, Dyesol). The electrolyte solution was inserted by vacuum backfilling. Then, the hole was sealed by using additional Surlyn patch and a cover glass and finally a conductive Ag-based paint was deposed at the electrical contacts.

The Iolitech ES-0004 HP electrolyte, containing 1butyl-3methylimidiazolium iodide, iodine, guanidinium thiocyanate and *tert*-butylpyridine, in a mixture of valeronitrile and acetonitrile was used for the I^-/I_3^- electrolyte reference cells. The effect of 0.1M of $LiClO_4$ was also tested. The cobalt-based electrolyte contains 0.2M $[Co(bpy)_3](PF_6)_2$, 0.02M $[Co(bpy)_3](PF_6)_3$, 0.1 M $LiClO_4$, and 0.5 M 4-tert-butylpyridine in acetonitrile. Where required, CDCA (Solaronix) was added to the electrolyte in 0.01M concentration. The employed amount of CDCA was not totally soluble in the cobalt electrolyte solution, so the mixture was stirred for 2h and the liquid fraction on the solution surface was used for the DSCs fabrication.

2.3 Photovoltaic Characterization

Photovoltaic measurements were recorded by means of AM 1.5 solar simulator equipped with a Xenon lamp (LOT-ORIEL LS 0106). The power of incoming radiation, set at 100 mW/cm^2, was checked by a piranometer. J–V curves were obtained by applying an external bias to the cell and measuring the generated photocurrent with a Keithley model 2400 digital source-meter, under the

control of dedicated LabTracer 2.0 software. A black shading mask was employed to avoid the overestimation of the measured parameters.[81]

2.4 FT-IR measurements

All the experimental spectra were recorded using a μ-FTIR instrument consisting of a JASCO® FTIR 4100 spectrometer, equipped with a liquid nitrogen cooled MCT detector coupled with an IMV-4000 optical microscope. Measurements were performed in transmission mode (through a Cassegrain 16X objective) on a micro diamond cell, scanning an energy range of 6000-600 cm^{-1} and with a resolution of 4 cm^{-1}. The spectra were recorded using 5000 scans; background correction was adopted by means of a spectrum collected on the empty micro diamond cell. TiO_2 precoated photoanodes, from Dyesol, were heated for 30min at 500°C. They were then dipped in a $2*10^{-2}$M solution of CDCA in solvent (EtOH, $CHCl_3$, Acetonitrile, from Baker, HPLC purity), overnight. After 20h they were rinsed with acetonitrile and a μ-FTIR spectrum of each sample was recorded directly on powders.

2.5 Computational details

The simulation of CDCA adsorption on the TiO_2 surface, was performed by means of the Car−Parrinello code, as implemented in the Quantum-Espresso package,[82] employing the GGA-PBE exchange-correlation functional[83] in combination with a plane wave basis set and ultrasoft pseudopotentials. Plane wave basis set cutoffs set for the smooth part of the wave functions and the augmented density are 25 and 200 Ry, respectively. The dimensions of the simulation supercells have been defined by adding 7 Å of vacuum to the largest dimension in each direction. Geometry optimization has been performed with a damped dynamics setting the atomic masses and the electronic fictitious to a value of 5 amu and 1500 a.u. with a time step simulation of 10 a.u. The electronic and ionic frictions have set to a values of 0.05 and 0.0007 a.u., respectively. The CP

geometries are further optimized with the ADF program package with the TZP basis-set for Ti atoms and DZP basis-set for the other atoms.

To model the TiO_2 surface, we consider a $(TiO_2)_{82}$ cluster, obtained by appropriately "cutting" an anatase slab exposing the majority (101) surface.[84] Following the work by Persson *et al.*,[85] we consider a neutral stoichiometric TiO_2 cluster with no saturating atoms or groups at the cluster border. These models have been shown to accurately reproduce the electronic and structural properties of TiO_2 anatase.[84] The calculated dipole moment for our $(TiO_2)_{82}$ cluster is correctly found to be almost vanishing in all directions (0.5, 0.7, and 0.8 D for x, y, and z, the latter corresponding to the surface normal). The employed $(TiO_2)_{82}$ model is an almost square TiO_2 (101) two-layer anatase slab of ~2 nm side, with three rows of five- and sixcoordinated surface Ti sites, which is large enough to avoid possible spurious dye/titania interactions at the cluster border due to the finite cluster size. Furthermore, Martsinovich *et al.* pointed out that TiO_2 anatase surface models are rather insensitive to the thickness of the TiO_2 layer,[86] with two layer slabs accurately reproducing the electronic and structural features of larger models. In addition to the vanishing dipole moment, the adequacy of the employed cluster model against periodic surface slabs has been further checked here by performing comparative CP calculations employing the same GGA functional employed for geometry optimizations.

CDCA molecules were adsorbed on TiO_2 in a bridged bi-dentate configuration.[13] To evaluate the possibility of CDCA aggregation in solution and on the semiconductor surface, we investigated the possible CDCA dimer and trimer formation calculating the association energy with the GGA-PBE approach and with the B3LYP hybrid functional[87] and solvation effects with the continuum polarizable model (PCM)[88, 89] as implemented in the Gaussian09[90] package program. The 6-31G* basis set[91] was used in all Gaussian calculation if not otherwise specified. Geometry optimization of the CDCA dimers have been also performed in solvent. The adsorption energy of the CDCA on to the TiO_2 cluster is calculated, from the total free energies in solution, as ΔE_{ads} =

$E(CDCA@TiO_2) - E(TiO_2) - E(CDCA)$ and the aggregation energy between two CDCA molecules is $\Delta E_{dim} = E(CDCA_2) - 2*E(CDCA)$.

3. Results and discussion

3.1 Photovoltaic Data

We start our discussion by a comparative investigation of the photovoltaic properties of DSC devices fabricated with the same photoanode/cathode but varying the dye (N719 or Z907) and the nature and composition of the electrolytes, see Table 1, Figures 1 and 2 and Supporting Information.

For devices based on the I^-/I_3^- reference electrolyte, the photovoltaic results with N719 and Z907 dyes are in line with the literature.[7] Notice that our fabrication protocol and the employed materials allow us to reproducibly obtain ~7% efficiency with ruthenium dyes and the I^-/I_3^- electrolyte, which therefore represents our benchmark performance.

Table 1. Photovoltaic parameters for DSCs employing different electrolytes and sensitizing dyes, measured under simulated AM 1.5 1 Sun illumination.

Cell	CDCA (dye)	CDCA (electrolyte)	$LiClO_4$	J_{sc} (mA/cm^2)	V_{oc} (mV)	FF	η (%)
I-Z907-1	No	No	No	13.0	780	0.64	6.5
I-Z907-2	0.02 M	0.01 M	No	12.3	780	0.69	6.6
I-Z907-3	No	No	0.1 M	14.5	721	0.61	6.4
I-Z907-4	0.02 M	0.01 M	0.1 M	14.6	724	0.65	6.9
Co-Z907-1	No	No	0.1 M	9.6	653	0.62	3.9
Co-Z907-2	0.02 M	0.01 M	0.1 M	11.8	732	0.61	5.3
Co-Z907-3	0.02 M	No	0.1 M	7.8	660	0.49	2.5
Co-Z907-4	No	0.01 M	0.1 M	7.6	669	0.57	2.9
I-N719-1	No	No	No	14.0	758	0.64	6.8
I-N719-2	0.02 M	0.01 M	No	13.2	780	0.67	6.9
I-N719-3	No	No	0.1 M	14.0	726	0.63	6.4
I-N719-4	0.02 M	0.01 M	0.1 M	14.2	758	0.63	6.8
Co-N719-1	No	No	0.1 M	2.1	332	0.43	0.3
Co-N719-2	0.02 M	0.01 M	0.1 M	5.4	651	0.68	2.4

Slightly better performances were obtained with N719 (I-N719-1) compared to the Z907 dye (I-Z907-1), due to a better photocurrent developed by N719-sensitized devices. By adding to the electrolyte the $LiClO_4$ additive (I-Z907-3 and I-N719-3), that is known to down-shift the TiO_2 conduction band,[92, 93] we note the expected increase of the short circuit photocurrent and a considerable reduction of the photovoltage, particularly in the case of DSCs sensitized with the

Z907 dye (see Figure 1a, 2a). Notice that, in line with the results of Ref. [11], addition of CDCA to the electrolyte solution does not have any particular influence on the photovoltaic performances of devices based on the I^-/I_3^- electrolyte.

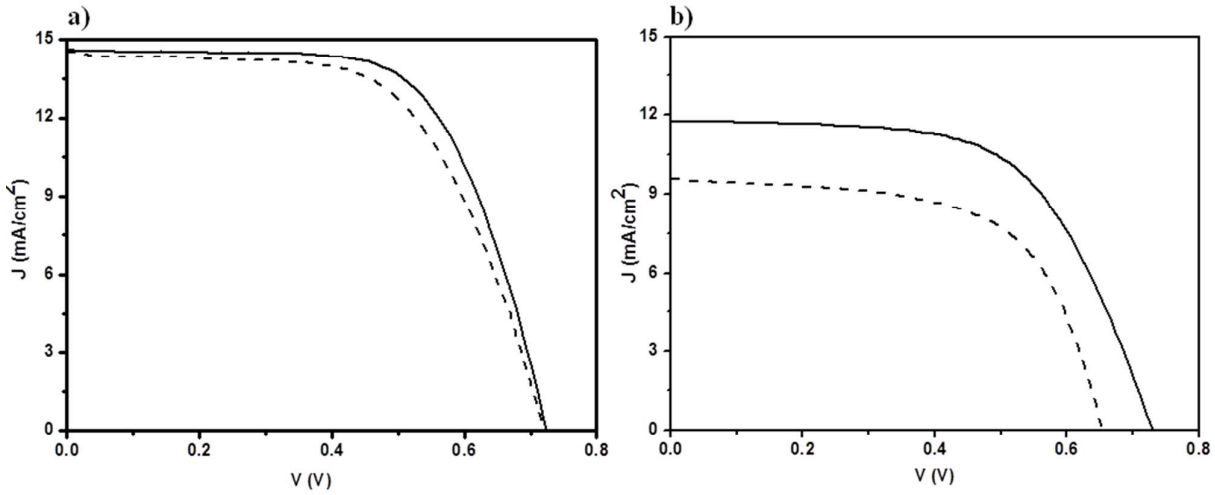

Figure 1. J-V characteristic of a) I-Z907-3 cell (dashed line) and I-Z907-4 (solid line) and b) Co-Z907-1 cell (dashed line) and Co-Z907-2 (solid line). Solid lines are referred to cells with CDCA additive both in dye solution (0.02M) and in the electrolyte (0.01M).

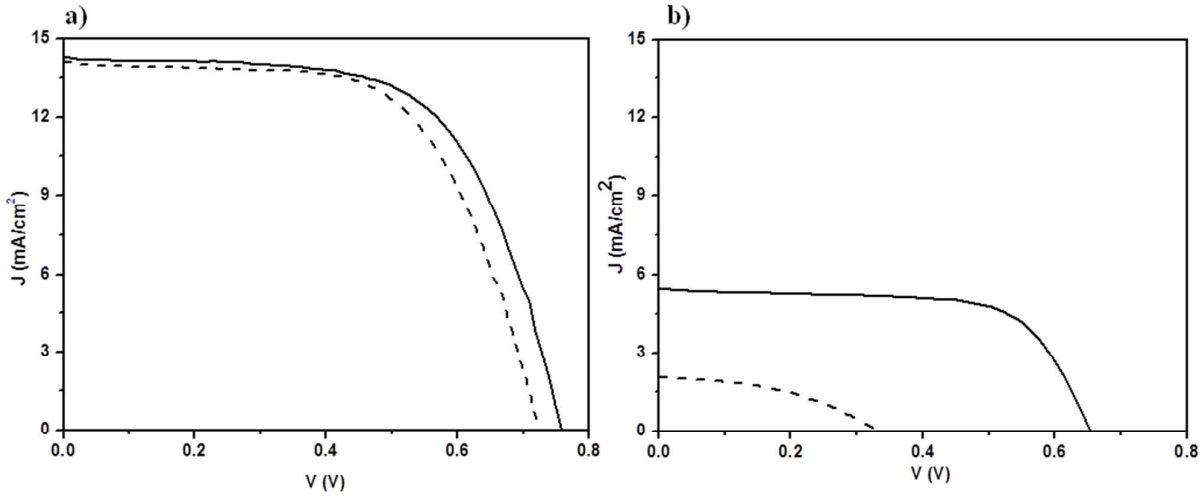

Figure 2. J-V characteristic of a) I-N719-3 cell (dashed line) and I-N719-4 (solid line) and b) Co-N719-1 cell (dashed line) and Co-N719-2 (solid line). Solid line are referred to cell with CDCA additive both in dye solution (0.02M) and in the electrolyte (0.01M).

Moving to the $[Co(bpy)_3]^{2+/3+}$ electrolyte, the photovoltaic parameters were strongly influenced both by the dye and the electrolyte composition. The Z907 dye (Co-Z907-1, Figure 1b) shows much better performances than N719 (Co-N719-1, Figure 2b) as previously found.[7, 60] This is mainly due to the steric hindrance introduced by the nonyl chains, which effectively insulate the TiO_2 surface reducing the recombination reactions. The poor performances of N719 highlight the important contribution of parasitic recombination reactions in limiting the device performance.[60] Since to obtain good results in combination with the $[Co(bpy)_3]^{2+/3+}$ electrolyte it seems of great importance to effectively shield the TiO_2 surface from the oxidized form of the redox couple, we tested the effect of the CDCA as an electrolyte additive, to check if the beneficial effect noted in the Fc/Fc^+ case[11] is verified also in the cobalt-based electrolyte.

For both Z907 and N719 dyes, when the CDCA was used both in the dye solution (0.02M) and in the electrolyte (nominally 0.01M), we obtained an impressive improvement of the device performances (Co-Z907-2 and Co-N719-2). In particular for the Z907 dye we were able to reach ~ 80% of the efficiency obtained for I^-/I_3^- based devices, passing from 3.9% to 5.3% conversion efficiency (see Table 1 and Figure 1). A significant gain of about 2 mA/cm^2 in J_{sc} and 80 mV in V_{oc} was obtained, testifying the effectiveness of the CDCA additive in reducing the recombination losses. It is worth noting that the extracted photovoltage in this case is slightly higher than that of the corresponding iodine-based DSCs using the same concentration of $LiClO_4$ (732 vs. 724 mV), in line with the higher (more positive) redox potential of $[Co(bpy)_3]^{2+/3+}$ electrolyte with respect to the I^-/I_3^-.[7] Obviously, our V_{oc} increase is still below the ideal ~ 100 mV gain that one would expect based on the difference in redox potentials of the two redox shuttles due to the possibly different

recombination kinetics in the two types of cells. Employing CDCA in the electrolyte solution, the photovoltaic performances of N719 still remain much lower compared to the corresponding Z907-based devices, although J_{sc} values of over 5 mA/cm^2 and V_{oc} of 0.65V were obtained, leading to an efficiency of 2.4% with this dye (Figure 2b). Slightly improved performance for N719-based DSCs (2.6 %) have been obtained using an opaque TiO_2 paste, which however led to a reduced efficiency (4.5 %) for Z907-based DSCs, see Supporting Information.

Further tests were conducted with the Z907 dye and the $[Co(bpy)_3]^{2+/3+}$ electrolyte, using CDCA alternatively in dye bath and in electrolyte solutions. In this case we obtained similar or reduced efficiency compared to devices not employing CDCA (Co-Z907-3 and Co-Z907-4). In both cases we noted a lower J_{sc} value, probably due to the competition of the CDCA with the dye for TiO_2 binding sites. The decrease of both parameters, added to quite poor FF values, led to a drop of the conversion efficiency of about 25% compared to the devices with no CDCA.

The fact that the improvement in photovoltaic efficiency has been obtained exclusively combining the CDCA additive in the dye bath *and* in the electrolyte solutions, is consistent with the formation of an equilibrium between the surface-adsorbed CDCA and the CDCA molecules in solution, as proposed by Daeneke *et al.* for the Fc/Fc^+ redox couple.[11] The presence of bulky CDCA assemblies onto or close to the TiO_2 surface, due to the possible establishment of supramolecular interactions among CDCA molecules, see below, could effectively limit the Co(III) ions approach to the semiconductor surface and the subsequent recombination with the injected electrons.

3.2 FT-IR spectra

As previously reported,[73-78] CDCA shows a strong intermolecular hydrogen bonding leading to an extended crystalline network in the solid state, see Figure 3. In particular, FT-IR measurements showed a characteristic peak of the hydrogen bonded C=O stretching, located at 1709 cm^{-1}.[77, 78]

Moving to the IR spectra in $CHCl_3$ solution, two signals at 1708 and 1742 cm^{-1} associated to the carbonyl group can be distinguished. Since the 1742 cm^{-1} signal is associated to the free C=O stretching, it has been proposed that, despite the solvent may break some intermolecular interactions, a kernel of CDCA molecules associated by hydrogen-bonding is present also in solution, showing the characteristic signal at 1709 cm^{-1} as in the solid state.[77, 78]

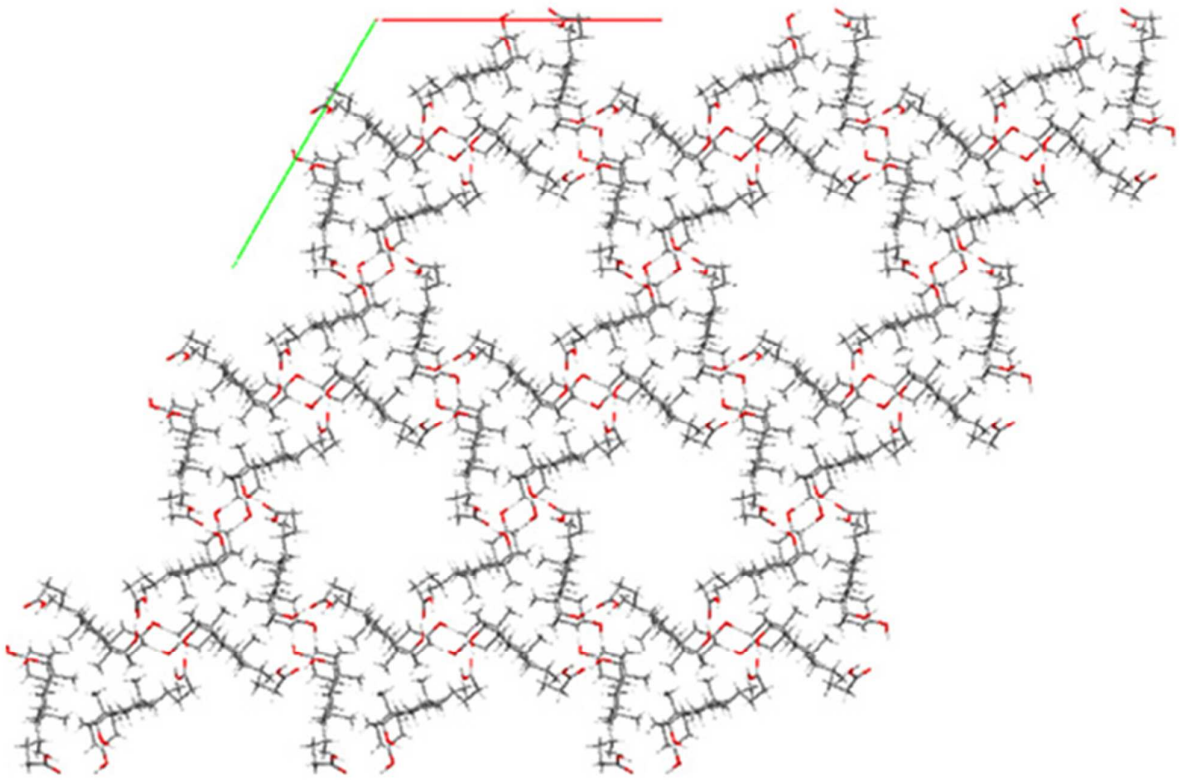

Figure 3. Crystal packing of CDCA molecules. Reprinted from Ref. [75], Steroids, 72, Alvarez, M.; Jover, A.; Carrazana, J.; Meijide, F.; Soto, V. H.; Tato, J. V. z., Crystal structure of chenodeoxycholic acid, ursodeoxycholic acid and their two 7d-dihydroxy epimers. Pages No. 535-544, Copyright (2007), with permission from Elsevier.

To check whether a similar aggregate structure could be maintained in our DSCs and to gain insight into the nature of these interactions at the TiO_2 surface, FT-IR measurements have been

carried out on solid CDCA and for CDCA adsorbed onto the semiconductor surface by applying the same procedure used for the DSCs device preparation.

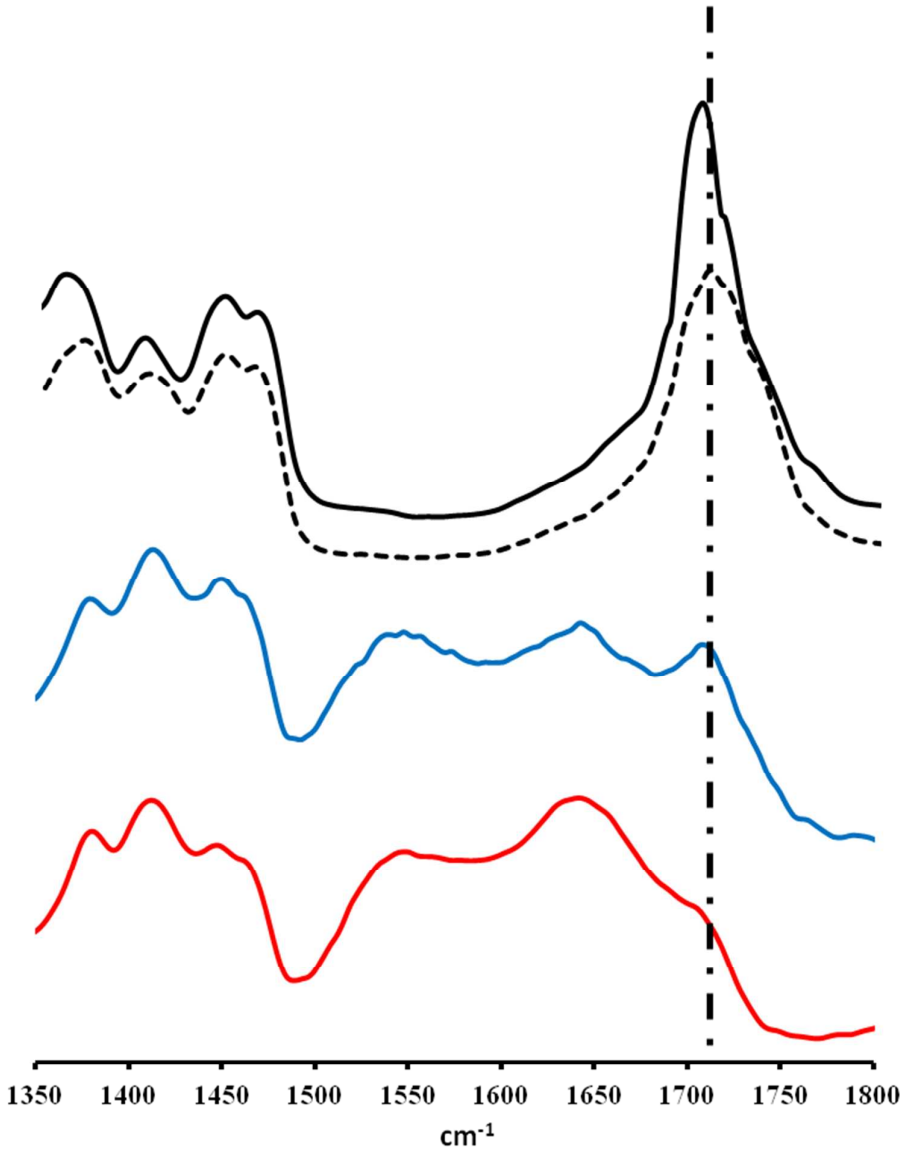

Figure 4. FT-IR absorption spectra of solid CDCA (black line); solid CDCA heated at 130 °C for 4 hours (black dashed line); CDCA adsorbed on TiO_2 from 0.02 M solutions in CH_3CN (blue line) and from EtOH (red line).

As we can see in Figure 4, the signals located at 1710 cm^{-1}, associated to the hydrogen bonded carboxylic stretching, are consistently found for the solid CDCA and for the TiO_2 surface-adsorbed CDCA, both from ethanol and acetonitrile solutions. The signals comprised in a range between 1550 to 1420 cm^{-1} are typical of the asymmetric and symmetric stretching of the TiO_2 surface-adsorbed CDCA carboxylate.[13] This presence of the signals of the surface-adsorbed carboxylate stretching and free carboxylic group confirms the permanence of an intermolecular aggregation pattern upon CDCA adsorption on TiO_2, of similar nature to what found in solid CDCA.

3.3 Computational analyses: Aggregate formation and interaction with TiO_2

Computational investigations have been carried out to tentatively assign the nature of the aggregates occurring for CDCA on the TiO_2 surface. In particular, the formation of CDCA hydrogen-bonded assemblies involving both the carboxylic acidic and the hydroxyl groups have been investigated. Here we adopt a stepwise procedure, and we initially simulate the aggregation of two CDCA molecules. On overall, we found four dimeric CDCA structures, Figure 5, characterized by the following interactions: i) hydrogen bonding between the two acidic (A) carboxylic moieties, $CDCA_2^{A/A}$; ii) hydrogen bonding between the hydroxyl (O) groups of both molecules, $CDCA_2^{O/O}$; iii) hydrogen bond between the carboxylic acid of one molecule and one OH group of the other molecule, $CDCA_2^{1O/A}$; and iv) hydrogen bond between the carboxylic acid of one molecule and both OH groups of the other molecule, $CDCA_2^{O/A}$.

As we can see in Table 2, the B3LYP binding energy values for the considered dimers are comprised between 19.6 and 13.4 kcal/mol in vacuo; these values reduce to 16.4-11.5 kcal/mol upon geometry optimization in acetonitrile solution. In all cases the $CDCA_2^{A/A}$ dimer is calculated as the most stable structure. The $CDCA_2^{O/O}$, $CDCA_2^{1O/A}$ and $CDCA_2^{O/A}$ structures are found within 1-2 kcal/mol, depending on the level of theory, and, considering data in solution, the second most

stable structure is found ca. 3 kcal/mol below the $CDCA_2^{A/A}$ dimer. These relevant values of aggregation energy suggest a strong tendency to form intermolecular interactions, in line with the experimental evidence.[71-74]

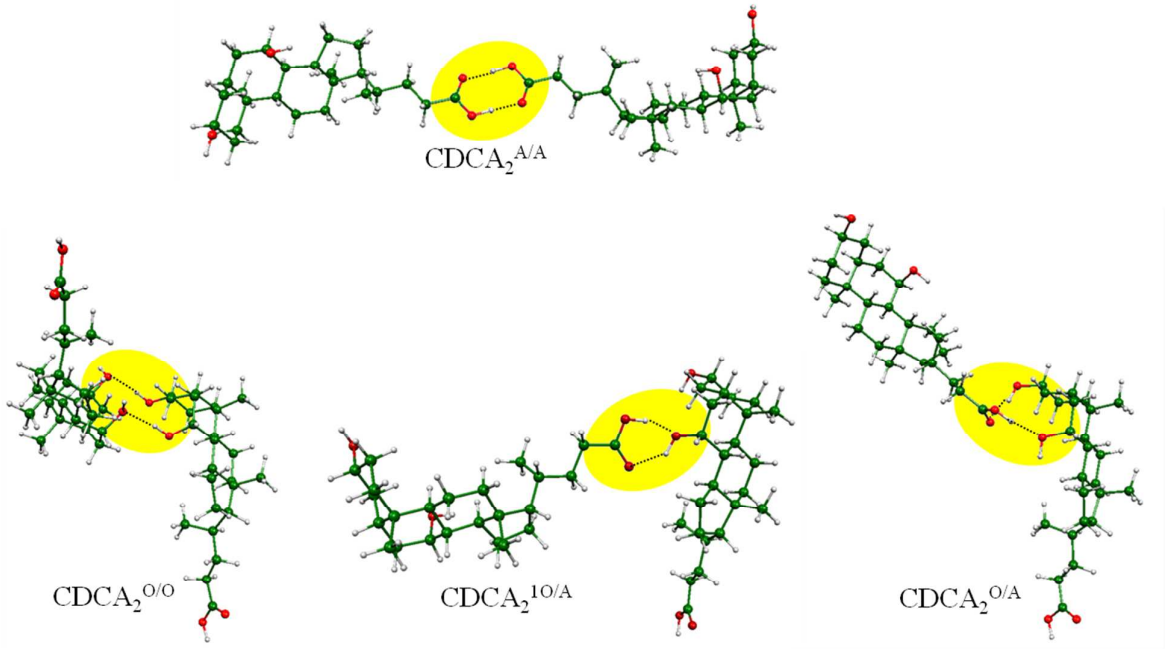

Figure 5. B3LYP-optimized geometries of the investigated CDCA dimers.

Table 2. Adsorption energies of CDCA and NKX2587 (ΔE_{ads}) in the bridged bidentate adsorption mode. Binding energy (ΔE_{dim}) of a series of CDCA dimers are also reported.

	System	ADF Geom.			G09 Geom.		
		PBE-GGA Vac.	B3LYP Vac.	B3LYP Solv.	Vac	Solv.	Opt. Solv.
ΔE_{ads} (kcal/mol)	NKX2587@TiO_2	-15.19	-22.02	-12.54	-	-	-
	CDCA@TiO_2	-14.08	-21.85	-15.46	-	-	-
ΔE_{dim} (kcal/mol)	$CDCA_2^{A/A}$	-21.65	-21.30	-17.34	-19.60	-15.42	-16.35
	$CDCA_2^{O/O}$	-14.73	-16.55	-14.44	-14.30	-11.96	-13.53
	$CDCA_2^{O/A}$	-13.30	-14.96	-12.48	-13.04	-10.08	-11.54
	$CDCA_2^{1O/A}$	-15.20	-14.52	-11.26	-14.88	-11.27	-12.49

The effect of the PBE-GGA functional on the geometry optimizations is also checked by relaxing the dimers with the ADF program package used for geometry optimizations of TiO_2-

adsorbed species. On these GGA geometries a single point energy with the B3LYP functional in vacuo and in solution has been carried out, demonstrating that the GGA geometries give a similar association energy if compared to the energy values obtain with the B3LYP optimized geometry, see Table 2. This observation allows us to optimize the CDCA adsorbed onto the $(TiO_2)_{82}$ nanocluster by GGA, thus reducing the computational cost, and then to evaluate the adsorption energies with a single point energy calculation at the B3LYP/PCM level.

The optimized geometries of CDCA adsorbed on TiO_2 is reported in Figure 6, along with that of the prototypical NKX2587 organic dye bearing a cyanoacrylic anchoring.[94] The TiO_2 adsorption energy of CDCA is 15.1 kcal/mol, essentially coinciding to the adsorption energy calculated for the NKX2587 dye (15.2 kcal/mol). This data confirms the possibility of a competition between the dye and the CDCA in binding to the TiO_2 semiconductor surface.

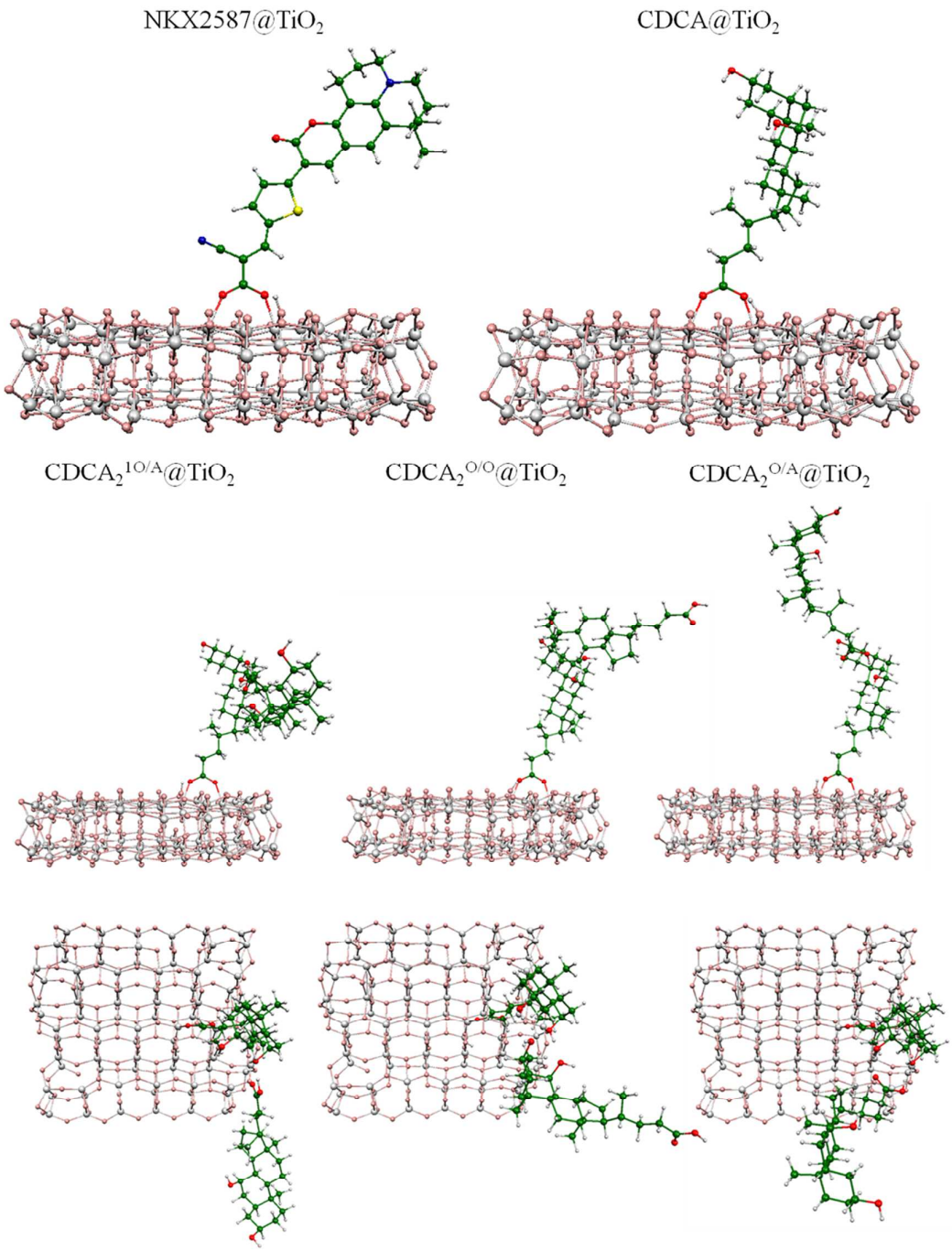

Figure 6. PBE-GGA geometries of the NKX2587, CDCA and $CDCA_2$ adsorbed on to the $(TiO_2)_{82}$ nanocluster in the bridged bidentate adsorption mode.

The adsorption energies of the various CDCA-CDCA dimers, apart from $CDCA_2^{A/A}$, are similar to the adsorption energy of a single CDCA molecule onto TiO_2, with values comprised between 13.3 and 15.2 kcal/mol. This data tells us that once one CDCA molecule is adsorbed on TiO_2, a comparable driving force occurs to bind a second CDCA molecule by hydrogen bonding or to bind a second CDCA molecule to TiO_2.

It is also interesting to evaluate the effect of CDCA adsorption on the TiO_2 conduction band (CB). Our data show that the position of the TiO_2 CB is not influenced by the presence of adsorbed CDCA in line with experimental measurements.[65] On the other hand the presence of the NKX2587 organic dye induces an energy up-shift of the TiO_2 CB by 0.08 eV, in line with our recent results.[95]

3.4 Simulation of IR spectra

Vibrational frequencies were calculated on the B3LYP optimized geometries for the various optimized aggregate configurations to simulate the IR spectra measured for CDCA in the solid state and in solution. As we can see in Figure 7, the experimental CDCA IR spectra measured after thermal treatment at 130° C for four hours shows a signal at 1705 cm^{-1} and a signal at 1709 cm^{-1}. These signals are in agreement with what previously reported in the literature[78] and are assigned to the C=O hydrogen bonded stretching of the carboxylic acid. As we can see in Figure 7, the calculated signal associated to the free C=O is located at ~ 1760 cm^{-1} for all the investigated species, see also Table 5 for a list of calculated frequencies. The $CDCA_2^{O/O}$ clearly shows only the signal associated to the hydrogen-bonded C=O stretching. On the other hand, the simulated IR spectra of the $CDCA_2^{O/A}$ and $CDCA_2^{1O/A}$ dimers show two signals with similar intensity. The signal located at 1705 cm^{-1} is associated to the stretching hydrogen-bonded C=O and the signal at 1762 cm^{-1} is associated the free C=O. The simulated spectra of the $CDCA_3^{1O/A}$ shows both hydrogen-bonded and free C=O signals (1709 and 1761 cm^{-1} respectively), where the intensity of the hydrogen-bonded C=O stretching is doubled with respect to the intensity of the free C=O. As we can see in Figure 7, going from the monomer to the trimer we have an increase of the intensity

of the hydrogen-bonded C=O stretching (while the intensity of the free C=O stretching decreases) and the simulated spectra seem to converge to the experimental signal of the C=O stretching obtained for the CDCA adsorbed onto the TiO_2 semiconductor. This suggests that a similar supramolecular aggregation may be occurring at the semiconductor surface.

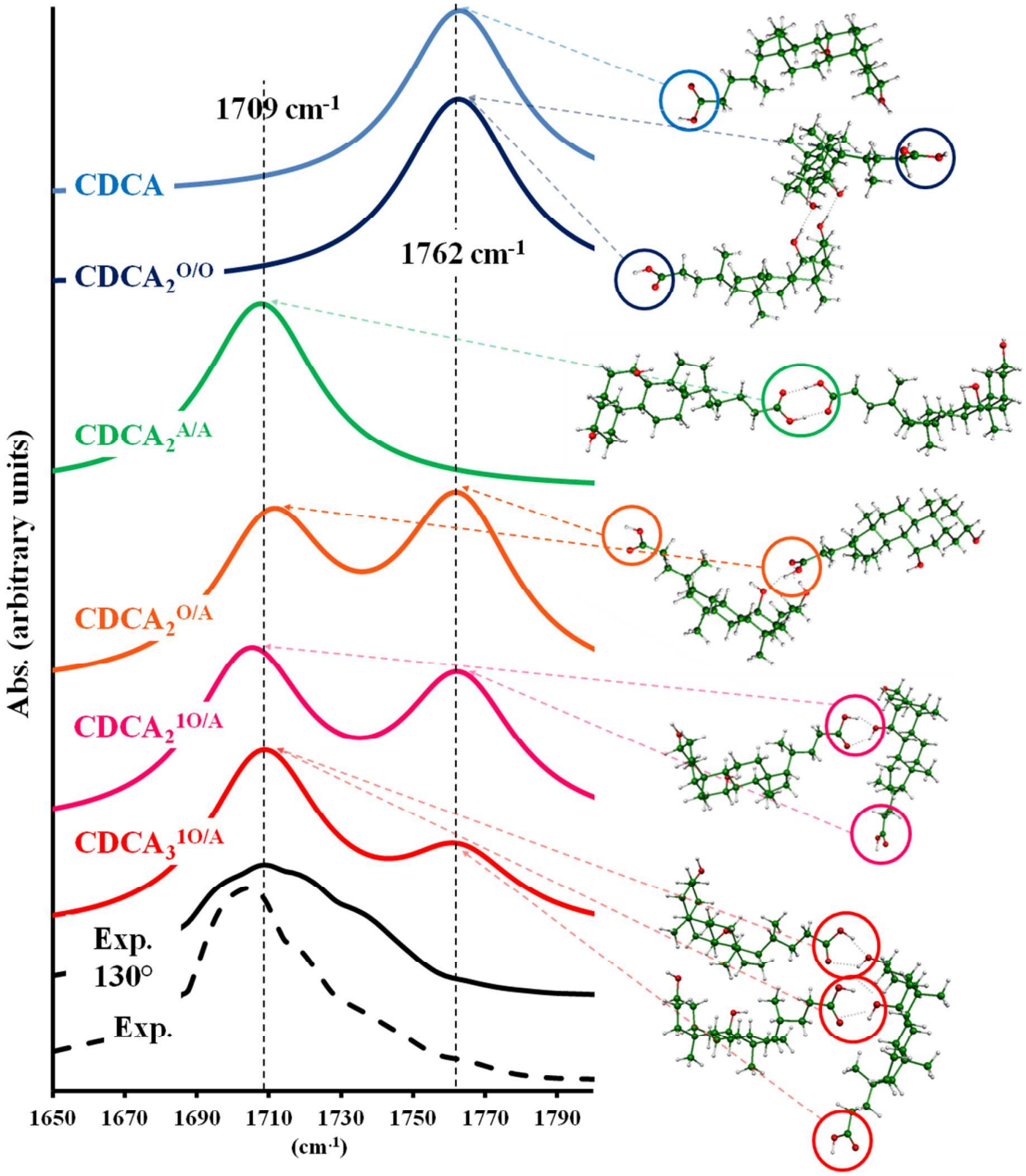

Figure 7. Comparison between the calculated IR spectra of the CDCA monomer (blue line), dimer

(magenta line) and trimer (red line) with the IR spectra measured for the CDCA at the solid state (black line). The calculated vibrational frequencies are scaled by 0.955.

As reported in the literature,[78] the IR spectra measured in $CHCl_3$ shows a signal at 1742 cm^{-1} which is assigned to the free C=O stretching. As we can see in Table 5, in the IR spectra of the $CDCA_2^{1O/A}$ dimer calculated in vacuo the free C=O stretching are located at higher frequencies (1761-1763 cm^{-1}) because of the absence of the solvent interactions. We thus also calculated the IR spectra in $CHCl_3$ solution for the $CDCA_2^{1O/A}$ dimer, which moves the C=O hydrogen-bonded stretching to match exactly with the experimental value (1708 cm^{-1}), see Table 5. By doing so also the C=O free stretching is shifted and is now calculated at 1756 cm^{-1} . This value is still higher compared to the experimental measurements, possibly because the continuum solvation approach does not reproduce the specific interaction with the solvent molecules. To improve the description of solute-solvent interactions, we further added a $CHCl_3$ solvent molecule close to the free carboxylic acid in the $CDCA_2^{1O/A}$ dimer obtaining a value of the C=O stretching of 1734 cm^{-1}, in closer agreement with the experimental data.

Table 5. Comparison between the calculated and experimental (this study) IR frequencies. [a] Values reported in ref [78].

Norm. Modes [cm^{-1}]		ν (C=O)		ν(O-H)			
		h. b.	free	h.b. alcol	h. b. acid	free acid	free alcol
Exp.	**Solid state**	**1705-1709** **1709** [a]	**-** **-**	**3426** [a] **-**	**-** **-**	**-** **-**	**-** **-**
Theor. Vac.	CDCA	-	1763	-	-	3519	3565-3587
	$CDCA_2^{1O/A}$	1705	1762	3410	3098	3519	3553-3564-3588
	$CDCA_3^{1O/A}$	1709	1761	3484-3488	3154-3230	3519	3563-3571-3589(2)
	$CDCA_2^{O/O}$	-	1763	3444	-	3520	(3579-3566)
	$CDCA_2^{O/A}$	1711	1763	3506	3262	3520	3565-3587 (3591)
	$CDCA_2^{A/A}$	1708	-	-	3078	-	3583(2)-3585(2)
Exp.	**Solution** [a]	**1708**	**1742**	**3520**		**3611**	**3690**

Theor. Solv.	$CDCA_2^{1O/A}$	1708	1756	3466	3093	3546	3598-3597-3617
	$CDCA_2^{1O/A}$ (+1 $CHCl_3$)	1708	1734	3462	3096	3506	3586-3596-3616

4. Conclusions

We have evaluated the combined effect of Chenodeoxycholic Acid (CDCA) as a surface co-adsorbent and as an additive in Dye-Sensitized Solar Cells based on a Co(II)/Co(III) electrolyte, in combination with the two prototypical Ru(II) dyes, i.e. N719 and Z907.

A comparative investigation of the photovoltaic properties of DSC devices fabricated varying the dye and the nature and composition of the electrolytes was performed. For devices based on the I^-/I_3^- reference electrolyte, the addition of CDCA to the electrolyte solution did not show any particular influence on the photovoltaic performances. Moving to the $[Co(bpy)_3]^{2+/3+}$ electrolyte, for both Z907 and N719 dyes, when the CDCA was used both in the dye solution and in the electrolyte, we obtained an impressive improvement of the device performances. In particular for the Z907 dye we were able to reach ~ 80% of the efficiency obtained for I^-/I_3^- based devices. A significant gain of about 2 mA/cm^2 in J_{sc} and 80 mV in V_{oc} was obtained, testifying the effectiveness of the CDCA additive in reducing the recombination losses. This results is in agreement with what reported by Daeneke et al.[11] for the related ferrocene/ferrocenium electrolyte.

The fact that the improvement in photovoltaic efficiency has been obtained exclusively combining the CDCA additive both in the dye bath *and* in the electrolyte solutions, suggests the possible formation of an equilibrium between the surface-adsorbed CDCA and the CDCA molecules in the electrolyte solution, which may reduce the Co(III) approach towards the TiO_2 surface, thus limiting unwanted recombination processes.

To check whether a CDCA aggregate structure similar to that found in the solid or in $CHCl_3$ solution could be maintained also in our DSCs and to gain insight into the nature of the supramolecular interaction at the sensitized-TiO_2 interface, FT-IR measurements have been carried

out on solid CDCA and when CDCA is adsorbed onto the TiO_2 semiconductor. Our analysis revealed the typical signals of the asymmetric and symmetrical stretching of the TiO_2 surface-adsorbed CDCA carboxylate, confirming that CDCA is anchored to the semiconductor, and at the same time the signal associated to the hydrogen bonded carboxylic stretching, confirming the permanence of a similar intermolecular aggregation in solid CDCA as well as upon TiO_2 adsorption.

To further clarify the nature of the supramolecular aggregates occurring for CDCA on the TiO_2 surface a series of computational investigations have been carried out. In particular, the formation of CDCA hydrogen-bonded assemblies involving both the carboxylic acidic function and the CDCA hydroxyl groups have been investigated. The binding energy calculated for the considered CDCA dimers are evaluated in a range of 19.6-3.4 and 16.4-11.5 kcal/mol in vacuo and in acetonitrile solution, respectively, suggesting a strong tendency to form intermolecular interactions. Moreover, the calculated TiO_2 adsorption energy of CDCA essentially coincides to that of the prototypical NKX2587 organic dye, confirming the possibility of a competition between the dye and the CDCA in anchoring to the TiO_2 semiconductor. Finally, by simulating the IR spectra of CDCA aggregates we found an increasing of the intensity of the hydrogen-bonded C=O stretching with a simultaneous decreasing of the free C=O stretching intensity and the simulated spectra seem to converge to the experimental measurements obtained for the CDCA adsorbed on to the TiO_2 semiconductor.

The overall picture extracted from our study suggests that the supramolecular aggregation of CDCA molecules is occurring also at the semiconductor surface, similar to what found in the solid and, to some extent, in solution. This aspect clearly leads to an increase of the device performance, which we associate to the formation of a network of CDCA molecules on or above the semiconductor surface. This CDCA network would probably insulate the TiO_2 surface limiting the approach of the oxidized Co(III) species and consequentially decreasing the effectiveness of

recombination processes between injected electrons and the oxidized cobalt electrolyte. A similar effect seems not to be at work in the case of I^-/I_3^- electrolyte, due to its much smaller dimensions and different chemical nature.

In conclusion, our study has shown that the beneficial effect of CDCA in the electrolyte solution on DSCs performance is not peculiar to the ferrocene/ferroccenium electrolyte but can be extended also to cobalt-based electrolytes. Simply by varying the composition of a cobalt-based electrolyte with a cheap and commercially available additive may further boost the efficiency of DSCs based on this redox mediator.

Acknowledgement: We thank FP7-ENERGY-2011 project 261920 "ESCORT" for financial support.

Supporting Information Available. J-V curves of the devices reported in Table 1, photovoltaic parameters and J-V curves of devices realized with a different TiO_2 paste. Full reference 90. This information is available free of charge via the Internet at http://pubs.acs.org .

REFERENCES

1. O'Regan, B.; Grätzel, M. A low-cost, high-efficiency solar cell based on dye-sensitized colloidal TiO_2 films. *Nature* **1991,** *353*,737-740.
2. Grätzel, M. Solar Energy Conversion by Dye-Sensitized Photovoltaic Cells. *Inorg. Chem.* **2005,** *44*,6841-6851.
3. Grätzel, M. Photoelectrochemical cells. *Nature* **2001,** *414*,338-344.
4. Grätzel, M. Recent Advances in Sensitized Mesoscopic Solar Cells. *Acc. Chem. Res.* **2009,** *42*,1788-1798.
5. Boschloo, G.; Hagfeldt, A. Characteristics of the Iodide/Triiodide Redox Mediator in Dye-Sensitized Solar Cells. *Acc. Chem. Res.* **2009,** *42*,1819-1826.
6. Feldt, S. M.; Gibson, E. A.; Gabrielsson, E.; Sun, L.; Boschloo, G.; Hagfeldt, A. Design of Organic Dyes and Cobalt Polypyridine Redox Mediators for High-Efficiency Dye-Sensitized Solar Cells. *J. Am. Chem. Soc.* **2010,** *132*,16714-16724.
7. Liu, Y.; Jennings, J. R.; Huang, Y.; Wang, Q.; Zakeeruddin, S. M.; Grätzel, M. Cobalt Redox Mediators for Ruthenium-Based Dye-Sensitized Solar Cells: A Combined Impedance Spectroscopy and Near-IR Transmittance Study. *J. Phys. Chem. C* **2011,** *115*,18847-18855.

8. Yella, A.; Lee, H.-W.; Tsao, H. N.; Yi, C.; Chandiran, A. K.; Nazeeruddin, M. K.; Diau, E. W.-G.; Yeh, C.-Y.; Zakeeruddin, S. M.; Grätzel, M. Porphyrin-Sensitized Solar Cells with Cobalt (II/III)-Based Redox Electrolyte Exceed 12 Percent Efficiency. *Science* **2011,** *334*,629-634.
9. Yum, J.-H.; Baranoff, E.; Kessler, F.; Moehl, T.; Ahmad, S.; Bessho, T.; Marchioro, A.; Ghadiri, E.; Moser, J.-E.; Yi, C., et al. A cobalt complex redox shuttle for dye-sensitized solar cells with high open-circuit potentials. *Nat. Commun.* **2012,** *3*,631-638.
10. Bai, Y.; Yu, Q.; Cai, N.; Wang, Y.; Zhang, M.; Wang, P. High-efficiency organic dye-sensitized mesoscopic solar cells with a copper redox shuttle. *Chem. Commun.* **2011,** *47*,4376-4378.
11. Daeneke, T.; Kwon, T.-H.; Holmes, A. B.; Duffy, N. W.; Bach, U.; Spiccia, L. High-efficiency dye-sensitized solar cells with ferrocene-based electrolytes. *Nat. Chem.* **2011,** *3*,1755-4330.
12. Daeneke, T.; Mozer, A. J.; Uemura, Y.; Makuta, S.; Fekete, M.; Tachibana, Y.; Koumura, N.; Bach, U.; Spiccia, L. Dye Regeneration Kinetics in Dye-Sensitized Solar Cells. *J. Am. Chem. Soc.* **2012,** *134*,16925-16928.
13. Anselmi, C.; Mosconi, E.; Pastore, M.; Ronca, E.; De Angelis, F. Adsorption of organic dyes on TiO_2 surfaces in dye-sensitized solar cells: interplay of theory and experiment. *Phys. Chem. Chem. Phys.* **2012,** *14*,15963-15974.
14. Anderson, S.; Constable, E. C.; Dare-Edwards, M. P.; Goodenough, J. B.; Hamnett, A.; Seddon, K. R.; Wright, R. D. Chemical modification of a titanium (IV) oxide electrode to give stable dye sensitisation without a supersensitiser. *Nature* **1979,** *280*,571-573.
15. Desilvestro, J.; Graetzel, M.; Kavan, L.; Moser, J.; Augustynski, J. Highly efficient sensitization of titanium dioxide. *J. Am. Chem. Soc.* **1985,** *107*,2988-2990.
16. Nazeeruddin, M. K.; Kay, A.; Rodicio, I.; Humphry-Baker, R.; Mueller, E.; Liska, P.; Vlachopoulos, N.; Grätzel, M. Conversion of light to electricity by cis-X_2bis(2,2'-bipyridyl-4,4'-dicarboxylate)ruthenium(II) charge-transfer sensitizers (X = Cl^-, Br^-, I^-, CN^-, and SCN^-) on nanocrystalline titanium dioxide electrodes. *J. Am. Chem. Soc.* **1993,** *115*,6382-6390.
17. Nazeeruddin, M. K.; Zakeeruddin, S. M.; Humphry-Baker, R.; Jirousek, M.; Liska, P.; Vlachopoulos, N.; Shklover, V.; Fischer, C.-H.; Grätzel, M. Acid-Base Equilibria of (2,2'-Bipyridyl-4,4'-dicarboxylic acid)ruthenium(II) Complexes and the Effect of Protonation on Charge-Transfer Sensitization of Nanocrystalline Titania. *Inorg. Chem.* **1999,** *38*,6298-6305.
18. K. Nazeeruddin, M.; Pechy, P.; Grätzel, M. Efficient panchromatic sensitization of nanocrystalline TiO2 films by a black dye based on a trithiocyanato-ruthenium complex. *Chem. Commun.* **1997,** *0*,1705-1706.
19. Nazeeruddin, M. K.; Pèchy, P.; Renouard, T.; Zakeeruddin, S. M.; Humphry-Baker, R.; Comte, P.; Liska, P.; Cevey, L.; Costa, E.; Shklover, V., et al. Engineering of Efficient Panchromatic Sensitizers for Nanocrystalline TiO_2-Based Solar Cells. *J. Am. Chem. Soc.* **2001,** *123*,1613-1624.
20. Han, L.; Islam, A.; Chen, H.; Malapaka, C.; Chiranjeevi, B.; Zhang, S.; Yang, X.; Yanagida, M. High-efficiency dye-sensitized solar cell with a novel co-adsorbent. *Energy Environ. Sci.* **2012,** *5*,6057-6060.
21. Nazeeruddin, M. K.; De Angelis, F.; Fantacci, S.; Selloni, A.; Viscardi, G.; Liska, P.; Ito, S.; Takeru, B.; Grätzel, M. Combined Experimental and DFT-TDDFT Computational Study of Photoelectrochemical Cell Ruthenium Sensitizers. *J. Am. Chem. Soc.* **2005,** *127*,16835-16847.
22. Wang, P.; Zakeeruddin, S. M.; Exnar, I.; Grätzel, M. High efficiency dye-sensitized nanocrystalline solar cells based on ionic liquid polymer gel electrolyte. *Chem. Commun.* **2002,** *0*,2972-2973.
23. Chen, C.-Y.; Wu, S.-J.; Wu, C.-G.; Chen, J.-G.; Ho, K.-C. A Ruthenium Complex with Superhigh Light-Harvesting Capacity for Dye-Sensitized Solar Cells. *Angew. Chem. Int. Ed.* **2006,** *45*,5822-5825.

24. Gao, F.; Wang, Y.; Shi, D.; Zhang, J.; Wang, M.; Jing, X.; Humphry-Baker, R.; Wang, P.; Zakeeruddin, S. M.; Grätzel, M. Enhance the Optical Absorptivity of Nanocrystalline TiO_2 Film with High Molar Extinction Coefficient Ruthenium Sensitizers for High Performance Dye-Sensitized Solar Cells. *J. Am. Chem. Soc.* **2008,** *130*,10720-10728.
25. Bessho, T.; Yoneda, E.; Yum, J.-H.; Guglielmi, M.; Tavernelli, I.; Imai, H.; Rothlisberger, U.; Nazeeruddin, M. K.; Grätzel, M. New Paradigm in Molecular Engineering of Sensitizers for Solar Cell Applications. *J. Am. Chem. Soc.* **2009,** *131*,5930-5934.
26. Bomben, P. G.; Koivisto, B. D.; Berlinguette, C. P. Cyclometalated Ru Complexes of Type $[Ru^{II}(N^N)_2(C\perp N)]^z$: Physicochemical Response to Substituents Installed on the Anionic Ligand. *Inorg. Chem.* **2010,** *49*,4960-4971.
27. Mishra, A.; Fischer, M. K. R.; Bäuerle, P. Metal-Free Organic Dyes for Dye-Sensitized Solar Cells: From Structure: Property Relationships to Design Rules. *Angew. Chem. Int. Ed.* **2009,** *48*,2474-2499.
28. Pastore, M.; Mosconi, E.; Fantacci, S.; De Angelis, F. Computational Investigations on Organic Sensitizers for Dye-Sensitized Solar Cells. *Curr. Org. Synth.* **2012,** *9*,215-232.
29. Zeng, W.; Cao, Y.; Bai, Y.; Wang, Y.; Shi, Y.; Zhang, M.; Wang, F.; Pan, C.; Wang, P. Efficient Dye-Sensitized Solar Cells with an Organic Photosensitizer Featuring Orderly Conjugated Ethylenedioxythiophene and Dithienosilole Blocks. *Chem. Mater.* **2010,** *22*,1915-1925.
30. Wu, S.-L.; Lu, H.-P.; Yu, H.-T.; Chuang, S.-H.; Chiu, C.-L.; Lee, C.-W.; Diau, E. W.-G.; Yeh, C.-Y. Design and characterization of porphyrin sensitizers with a push-pull framework for highly efficient dye-sensitized solar cells. *Energ Environ. Sci.* **2010,** *3*,949-955.
31. Chang, Y.-C.; Wang, C.-L.; Pan, T.-Y.; Hong, S.-H.; Lan, C.-M.; Kuo, H.-H.; Lo, C.-F.; Hsu, H.-Y.; Lin, C.-Y.; Diau, E. W.-G. A strategy to design highly efficient porphyrin sensitizers for dye-sensitized solar cells. *Chem. Commun.* **2011,** *47*,8910-8912.
32. Ito, S.; Chen, P.; Comte, P.; Nazeeruddin, M. K.; Liska, P.; Péchy, P.; Grätzel, M. Fabrication of screen-printing pastes from TiO_2 powders for dye-sensitised solar cells. *Prog. Photovolt.: Res. Appl.* **2007,** *15*,603-612.
33. Zhang, Z.; Ito, S.; O'Regan, B.; Kuang, D.; Zakeeruddin, S. M.; Liska, P.; Charvet, R. l.; Comte, P.; Nazeeruddin, M. K.; Pèchy, P., et al. The Electronic Role of the TiO_2 Light-Scattering Layer in Dye-Sensitized Solar Cells. *Z. Phys. Chem.* **2007,** *221*,319-327.
34. Shankar, K.; Gopal, K. M.; Prakasam, H. E.; Paulose, S. Y. M.; Varghese, O. K.; Grimes, C. A. Highly-ordered TiO_2 nanotube arrays up to 220 μm in length: use in water photoelectrolysis and dye-sensitized solar cells. *Nanotech.* **2007,** *18*,065707.
35. Saito, M.; Fujihara, S. Large photocurrent generation in dye-sensitized ZnO solar cells. *Energy Environ. Sci.* **2008,** *1*,280-283.
36. Keis, K.; Lindgren, J.; Lindquist, S.-E.; Hagfeldt, A. Studies of the Adsorption Process of Ru Complexes in Nanoporous ZnO Electrodes. *Langmuir* **2000,** *16*,4688-4694.
37. Anta, J. A.; Guillèn, E.; Tena-Zaera, R. ZnO-Based Dye-Sensitized Solar Cells. *J. Phys. Chem. C* **2012,** *116*,11413-11425.
38. Ferrere, S.; Zaban, A.; Gregg, B. A. Dye Sensitization of Nanocrystalline Tin Oxide by Perylene Derivatives. *J. Phys. Chem. B* **1997,** *101*,4490-4493.
39. Kay, A.; Grätzel, M. Dye-Sensitized Core-Shell Nanocrystals: Improved Efficiency of Mesoporous Tin Oxide Electrodes Coated with a Thin Layer of an Insulating Oxide. *Chem. Mater.* **2002,** *14*,2930-2935.
40. Snaith, H. J.; Moule, A. J.; Klein, C. d.; Meerholz, K.; Friend, R. H.; Grätzel, M. Efficiency Enhancements in Solid-State Hybrid Solar Cells via Reduced Charge Recombination and Increased Light Capture. *Nano Lett.* **2007,** *7*,3372-3376.

41. Cai, N.; Moon, S.-J.; Cevey-Ha, L.; Moehl, T.; Humphry-Baker, R.; Wang, P.; Zakeeruddin, S. M.; Grätzel, M. An Organic D-π-A Dye for Record Efficiency Solid-State Sensitized Heterojunction Solar Cells. *Nano Lett.* **2011,** *11*,1452-1456.
42. O'Regan, B. C.; Durrant, J. R. Kinetic and Energetic Paradigms for Dye-Sensitized Solar Cells: Moving from the Ideal to the Real. *Acc. Chem. Res.* **2009,** *42*,1799-1808.
43. Gregg, B. A.; Pichot, F. o.; Ferrere, S.; Fields, C. L. Interfacial Recombination Processes in Dye-Sensitized Solar Cells and Methods To Passivate the Interfaces. *J. Phys. Chem. B* **2001,** *105*,1422-1429.
44. Nusbaumer, H.; Moser, J.-E.; Zakeeruddin, S. M.; Nazeeruddin, M. K.; Grätzel, M. $Co^{II}(dbbip)_2^{2+}$ Complex Rivals Tri-iodide/Iodide Redox Mediator in Dye-Sensitized Photovoltaic Cells. *J. Phys. Chem. B* **2001,** *105*,10461-10464.
45. Sapp, S. A.; Elliott, C. M.; Contado, C.; Caramori, S.; Bignozzi, C. A. Substituted Polypyridine Complexes of Cobalt(II/III) as Efficient Electron-Transfer Mediators in Dye-Sensitized Solar Cells. *J. Am. Chem. Soc.* **2002,** *124*,11215-11222.
46. Nusbaumer, H.; Zakeeruddin, S. M.; Moser, J.-E.; Grätzel, M. An Alternative Efficient Redox Couple for the Dye-Sensitized Solar Cell System. *Chem. Eur. J.* **2003,** *9*,3756-3763.
47. Cameron, P. J.; Peter, L. M.; Zakeeruddin, S. M.; Grätzel, M. Electrochemical studies of the Co(III)/Co(II)$(dbbip)_2$ redox couple as a mediator for dye-sensitized nanocrystalline solar cells. *Coord. Chem. Rev.* **2004,** *248*,1447-1453.
48. Wang, H.; Nicholson, P. G.; Peter, L.; Zakeeruddin, S. M.; Grätzel, M. Transport and Interfacial Transfer of Electrons in Dye-Sensitized Solar Cells Utilizing a $Co(dbbip)_2$ Redox Shuttle. *J. Phys. Chem. C* **2010,** *114*,14300-14306.
49. Feldt, S. M.; Wang, G.; Boschloo, G.; Hagfeldt, A. Effects of Driving Forces for Recombination and Regeneration on the Photovoltaic Performance of Dye-Sensitized Solar Cells using Cobalt Polypyridine Redox Couples. *J. Phys. Chem. C* **2011,** *115*,21500-21507.
50. Tsao□, H. N.; Yi□, C.; Moehl, T.; Yum, J.-H.; Zakeeruddin, S. M.; Nazeeruddin, M. K.; Grätzel, M. Cyclopentadithiophene Bridged Donor–Acceptor Dyes Achieve High Power Conversion Efficiencies in Dye-Sensitized Solar Cells Based on the tris-Cobalt Bipyridine Redox Couple. *ChemSusChem* **2011,** *4*,591-594.
51. Hamann, T. W.; Farha, O. K.; Hupp, J. T. Outer-Sphere Redox Couples as Shuttles in Dye-Sensitized Solar Cells. Performance Enhancement Based on Photoelectrode Modification via Atomic Layer Deposition. *J. Phys. Chem. C* **2008,** *112*,19756-19764.
52. Feldt, S. M.; Cappel, U. B.; Johansson, E. M. J.; Boschloo, G.; Hagfeldt, A. Characterization of Surface Passivation by Poly(methylsiloxane) for Dye-Sensitized Solar Cells Employing the Ferrocene Redox Couple. *J. Phys. Chem. C* **2010,** *114*,10551-10558.
53. Hattori, S.; Wada, Y.; Yanagida, S.; Fukuzumi, S. Blue Copper Model Complexes with Distorted Tetragonal Geometry Acting as Effective Electron-Transfer Mediators in Dye-Sensitized Solar Cells. *J. Am. Chem. Soc.* **2005,** *127*,9648-9654.
54. Zhang, Z.; Chen, P.; Murakami, T. N.; Zakeeruddin, S. M.; Grätzel, M. The 2,2,6,6-Tetramethyl-1-piperidinyloxy Radical: An Efficient, Iodine- Free Redox Mediator for Dye-Sensitized Solar Cells. *Adv. Funct. Mater.* **2008,** *18*,341-346.
55. Wang, M.; Chamberland, N.; Breau, L.; Moser, J.-E.; Humphry-Baker, R.; Marsan, B. t.; Zakeeruddin, S. M.; Grätzel, M. An organic redox electrolyte to rival triiodide/iodide in dye-sensitized solar cells. *Nat. Chem.* **2010,** *2*,385-389.
56. O'Regan, B.; Schwartz, D. T. Efficient Photo-Hole Injection from Adsorbed Cyanine Dyes into Electrodeposited Copper(I) Thiocyanate Thin Films. *Chem. Mater.* **1995,** *7*,1349-1354.
57. O'Regan, B. C.; Lenzmann, F. Charge Transport and Recombination in a Nanoscale Interpenetrating Network of n-Type and p-Type Semiconductors: Transient Photocurrent and

Photovoltage Studies of TiO_2/Dye/CuSCN Photovoltaic Cells. *J. Phys. Chem. B* **2004,** *108*,4342-4350.
58. Chakrapani, V.; Baker, D.; Kamat, P. V. Understanding the Role of the Sulfide Redox Couple (S^{2-}/S_n^{2-}) in Quantum Dot-Sensitized Solar Cells. *J. Am. Chem. Soc.* **2011,** *133*,9607-9615.
59. Jovanovski, V.; Gonzàlez-Pedro, V.; Gimènez, S.; Azaceta, E.; Cabañero, G. n.; Grande, H.; Tena-Zaera, R.; Mora-Serò, I.; Bisquert, J. A Sulfide/Polysulfide-Based Ionic Liquid Electrolyte for Quantum Dot-Sensitized Solar Cells. *J. Am. Chem. Soc.* **2011,** *133*,20156-20159.
60. Mosconi, E.; Yum, J.-H.; Kessler, F.; Gòmez Garcìa, C. J.; Zuccaccia, C.; Cinti, A.; Nazeeruddin, M. K.; Grätzel, M.; De Angelis, F. Cobalt Electrolyte/Dye Interactions in Dye-Sensitized Solar Cells: A Combined Computational and Experimental Study. *J. Am. Chem. Soc.* **2012,** *134*,19438-19453.
61. Kay, A.; Grätzel, M. Artificial photosynthesis. 1. Photosensitization of titania solar cells with chlorophyll derivatives and related natural porphyrins. *J. Phys. Chem.* **1993,** *97*,6272-6277.
62. Hara, K.; Dan-oh, Y.; Kasada, C.; Ohga, Y.; Shinpo, A.; Suga, S.; Sayama, K.; Arakawa, H. Effect of Additives on the Photovoltaic Performance of Coumarin-Dye-Sensitized Nanocrystalline TiO_2 Solar Cells. *Langmuir* **2004,** *20*,4205-4210.
63. Lee, K.-M.; Suryanarayanan, V.; Ho, K.-C.; Justin Thomas, K. R.; Lin, J. T. Effects of co-adsorbate and additive on the performance of dye-sensitized solar cells: A photophysical study. *Sol. En. Mater. Sol. Cells* **2007,** *91*,1426-1431.
64. Yum, J. H.; Moon, S. J.; Humphry-Baker, R.; Walter, P.; Geiger, T.; Nüesch, F.; Grätzel, M.; Nazeeruddin, M. d. K. Effect of coadsorbent on the photovoltaic performance of squaraine sensitized nanocrystalline solar cells. *Nanotechnology* **2008,** *19*,424005.
65. Yum, J.-H.; Jang, S.; Humphry-Baker, R.; Grätzel, M.; Cid, J.-J.; Torres, T.; Nazeeruddin, M. K. Effect of Coadsorbent on the Photovoltaic Performance of Zinc Pthalocyanine-Sensitized Solar Cells. *Langmuir* **2008,** *24*,5636-5640.
66. Lu, H.-P.; Tsai, C.-Y.; Yen, W.-N.; Hsieh, C.-P.; Lee, C.-W.; Yeh, C.-Y.; Diau, E. W.-G. Control of Dye Aggregation and Electron Injection for Highly Efficient Porphyrin Sensitizers Adsorbed on Semiconductor Films with Varying Ratios of Coadsorbate. *J. Phys. Chem. C* **2009,** *113*,20990-20997.
67. Jiang, X.; Marinado, T.; Gabrielsson, E.; Hagberg, D. P.; Sun, L.; Hagfeldt, A. Structural Modification of Organic Dyes for Efficient Coadsorbent-Free Dye-Sensitized Solar Cells. *J. Phys. Chem. C* **2010,** *114*,2799-2805.
68. Ehret, A.; Stuhl, L.; Spitler, M. T. Spectral Sensitization of TiO_2 Nanocrystalline Electrodes with Aggregated Cyanine Dyes. *J. Phys. Chem. B* **2001,** *105*,9960-9965.
69. Tatay, S.; Haque, S. A.; O'Regan, B.; Durrant, J. R.; Verhees, W. J. H.; Kroon, J. M.; Vidal-Ferran, A.; Gavina, P.; Palomares, E. Kinetic competition in liquid electrolyte and solid-state cyanine dye sensitized solar cells. *J. Mater. Chem.* **2007,** *17*,3037-3044.
70. Wang, Z.-S.; Cui, Y.; Dan-oh, Y.; Kasada, C.; Shinpo, A.; Hara, K. Thiophene-Functionalized Coumarin Dye for Efficient Dye-Sensitized Solar Cells: Electron Lifetime Improved by Coadsorption of Deoxycholic Acid. *J. Phys. Chem. C* **2007,** *111*,7224-7230.
71. Pastore, M.; De Angelis, F. Aggregation of Organic Dyes on TiO_2 in Dye-Sensitized Solar Cells Models: An ab Initio Investigation. *ACS Nano* **2009,** *4*,556-562.
72. Bauer, C.; Boschloo, G.; Mukhtar, E.; Hagfeldt, A. Interfacial Electron-Transfer Dynamics in Ru(tcterpy)$(NCS)_3$-Sensitized TiO_2 Nanocrystalline Solar Cells. *J. Phys. Chem. B* **2002,** *106*,12693-12704.
73. Lindley, P. F.; Mahmoud, M. M.; Watson, F. E.; Jones, W. A. The structure of chenodeoxycholic acid $C_{24}H_{40}O_4$. *Acta Cryst. B* **1980,** *36*,1893-1897.

74. Rizkallah, P. J.; Harding, M. M.; Lindley, P. F.; Aigner, A.; Bauer, A. Structure of a low-temperature polymorph of chenodeoxycholic acid, $C_{24}H_{40}O_4$, determined with synchrotron radiation. *Acta Cryst. B* **1990,** *46*,262-266.
75. Alvarez, M.; Jover, A.; Carrazana, J.; Meijide, F.; Soto, V. H.; Tato, J. V. z. Crystal structure of chenodeoxycholic acid, ursodeoxycholic acid and their two 3β,7α and 3β,7β-dihydroxy epimers. *Steroids* **2007,** *72*,535-544.
76. Oguchi, T.; Sasaki, N.; Hara, T.; Tozuka, Y.; Yamamoto, K. Differentiated thermal crystallization from amorphous chenodeoxycholic acid between the ground specimens derived from the polymorphs. *Int. J. Pharm.* **2003,** *253*,81-88.
77. Lamcharfi, E.; Cohen-Solal, C.; Parquet, M.; Lutton, C.; Duprè, J.; Meyer, C. Determination of molecular associations of some hydrophobic and hydrophilic bile acids by infrared and Raman spectroscopy. *Eur. Biophys. J.* **1997,** *25*,285-291.
78. Lamcharfi, L.; Meyer, C.; Lutton, C. Rationalization of the relative hydrophobicity of some common bile acids by infrared and Raman spectroscopy. *Biospectroscopy* **1997,** *3*,393-401.
79. Planells, M.; Cespedes-Guirao, F. J.; Goncalves, L.; Sastre-Santos, A.; Fernandez-Lazaro, F.; Palomares, E. Supramolecular interactions in dye-sensitised solar cells. *J. Mater. Chem.* **2009,** *19*,5818-5825.
80. Planells, M.; Gonzàlez, A.; Ballester, P.; Palomares, E. Influencing parameters for the achievement of porphyrin supramolecular architectures on mesoporous metal oxide nanoparticles. *J. Porphyrins Phthalocyanines* **2011,** *15*,592-597.
81. Ito, S.; Nazeeruddin, M. K.; Liska, P.; Comte, P.; Charvet, R.; Péchy, P.; Jirousek, M.; Kay, A.; Zakeeruddin, S. M.; Grätzel, M. Photovoltaic characterization of dye-sensitized solar cells: effect of device masking on conversion efficiency. *Progr. Photovolt.: Res. Appl.* **2006,** *14*,589-601.
82. Giannozzi, P.; Baroni, S.; Bonini, N.; Calandra, M.; Car, R.; Cavazzoni, C.; Ceresoli, D.; Guido, L. C.; Cococcioni, M.; Dabo, I., et al. QUANTUM ESPRESSO: a modular and open-source software project for quantum simulations of materials. *J. Phys.: Condens. Matter* **2009,** *21*,395502.
83. Perdew, J. P.; Burke, K.; Ernzerhof, M. Generalized Gradient Approximation Made Simple. *Phys. Rev. Lett.* **1996,** *77*,3865-3868.
84. Vittadini, A.; Selloni, A.; Rotzinger, F. P.; Gr□tzel, M. Structure and Energetics of Water Adsorbed at TiO_2 Anatase \(101\) and \(001\) Surfaces. *Phys. Rev. Lett.* **1998,** *81*,2954-2957.
85. Lundqvist, M. J.; Nilsing, M.; Persson, P.; Lunell, S. DFT study of bare and dye-sensitized TiO_2 clusters and nanocrystals. *Int. J. Quantum Chem.* **2006,** *106*,3214-3234.
86. Martsinovich, N.; Jones, D. R.; Troisi, A. Electronic Structure of TiO2 Surfaces and Effect of Molecular Adsorbates Using Different DFT Implementations. *J. Phys. Chem. C* **2010,** *114*,22659-22670.
87. Becke, A. D. Density‐functional thermochemistry. III. The role of exact exchange. *J. Chem. Phys.* **1993,** *98*,5648-5652.
88. Cossi, M.; Barone, V. Time-dependent density functional theory for molecules in liquid solutions. *J. Chem. Phys.* **2001,** *115*,4708-4717.
89. Cossi, M.; Rega, N.; Scalmani, G.; Barone, V. Energies, structures, and electronic properties of molecules in solution with the C-PCM solvation model. *J. Comput. Chem.* **2003,** *24*,669-681.
90. Frisch, M. J.; Trucks, G. W.; Schlegel, H. B.; Scuseria, G. E.; Robb, M. A.; Cheeseman, J. R.; Montgomery, J. A. Jr.; Vreven, T.; Kudin, K. N.; Burant, J. C.; et al. Gaussian 09. Rev. B2. *Gaussian, Inc.*, Wallingford CT, 2009. See Supporting Information for full reference.
91. Ditchfield, R.; Hehre, W. J.; Pople, J. A. Self-Consistent Molecular-Orbital Methods. IX. An Extended Gaussian-Type Basis for Molecular-Orbital Studies of Organic Molecules. *J. Chem. Phys.* **1971,** *54*,724-728.
92. Redmond, G.; Fitzmaurice, D. Spectroscopic determination of flatband potentials for polycrystalline titania electrodes in nonaqueous solvents. *J. Phys. Chem.* **1993,** *97*,1426-1430.

93. Fredin, K.; Nissfolk, J.; Boschloo, G.; Hagfeldt, A. The influence of cations on charge accumulation in dye-sensitized solar cells. *J. Electroanal. Chem.* **2007,** *609*,55-60.
94. Miyashita, M.; Sunahara, K.; Nishikawa, T.; Uemura, Y.; Koumura, N.; Hara, K.; Mori, A.; Abe, T.; Suzuki, E.; Mori, S. Interfacial Electron-Transfer Kinetics in Metal-Free Organic Dye-Sensitized Solar Cells: Combined Effects of Molecular Structure of Dyes and Electrolytes. *J. Am. Chem. Soc.* **2008,** *130*,17874-17881.
95. Ronca, E.; Pastore, M.; Belpassi, L.; Tarantelli, F.; De Angelis, F. Influence of the dye molecular structure on the TiO_2 conduction band in dye-sensitized solar cells: disentangling charge transfer and electrostatic effects. *Energy Environ. Sci.* **2013,** *6*,183-193.

SYNOPSIS TOC